On the nature of short-period mesospheric gravity wave propagation over Halley, Antarctica

K. Nielsen,[1] M. J. Taylor,[2] R. E. Hibbins,[3,4] M. J. Jarvis,[3] and J. M. Russell III[5]

Received 17 May 2011; revised 1 January 2012; accepted 3 January 2012; published 10 March 2012.

[1] As part of a collaborative program between British Antarctic Survey and Utah State University, measurements were made using an all-sky airglow imager located at the U.K. Halley Station (76°S, 27°W) during the 2000 and 2001 austral winter seasons from April through to early September. A co-located imaging Doppler interferometer was utilized to obtain coincident wind measurements for a total of 171 wave events. This study comprises the first detailed climatological investigation of the propagation nature (freely propagating, Doppler ducted, or evanescent) of individual quasi-monochromatic, short-period wave events at a high southern latitude. Distributions of the derived vertical wavelength exhibit an interquartile range from ∼16–48 km with a median vertical wavelength of 21 km. The majority of the wave events were found to be freely propagating waves, with only ∼5% exhibiting a clear Doppler ducted signature, while 15% of the waves were found to be evanescent in nature. Although no coincident temperature measurements were available, subsequent SABER temperature measurements suggest that up to ∼28% of the measured temperature profiles are capable of providing a ducted environment for the observed wave field. This is in sharp contrast to findings at mid- and low latitudes where these waves have been shown to be prone to Doppler ducted motion. It is suggested that the relatively weak wind field and associated tidal wind amplitudes over Halley are not capable of forming a significant Doppler ducted region to sustain a substantial amount of ducted waves belonging to the detectable spectrum of the airglow imager. As these wind fields are comparable to wind fields found at other polar latitudes, we hypothesize that the majority of short-period gravity waves observed in the polar mesosphere are freely propagating and thus an important source of energy transfer into the MLT region.

Citation: Nielsen, K., M. J. Taylor, R. E. Hibbins, M. J. Jarvis, and J. M. Russell III (2012), On the nature of short-period mesospheric gravity wave propagation over Halley, Antarctica, *J. Geophys. Res.*, *117*, D05124, doi:10.1029/2011JD016261.

1. Introduction

[2] Gravity waves, particularly short-period, fast moving events, can propagate rapidly from their tropospheric source region into the Mesosphere and Lower Thermosphere (MLT) region where they saturate and break, depositing significant amounts of momentum (see review by *Fritts and Alexander* [2003, and references therein]). Indeed, it has been shown that as much as 70% of the momentum transported into the MLT region is due to short-period (<1-hr) gravity waves penetrating into this region from below [*Fritts and Vincent*, 1987]. The impact by these waves on the MLT region is of great significance as modeling studies have shown that the momentum deposited reverses the mesospheric wind jet and is a major factor in the formation of the unexpectedly cold summer mesopause region at high latitudes [*Fritts and Alexander*, 2003].

[3] An all-sky (180°) airglow imager was deployed at Halley Station, Antarctica (76°S, 27°W) during the 2000 and 2001 austral winter seasons as a collaborative effort between the British Antarctic Survey (BAS) and Utah State University (USU) to study short-period gravity waves at high latitudes. In addition, a Dynasonde/Imaging Doppler Interferometer (IDI) instrument [*Jones et al.*, 1997] co-located at Halley has been used to observe mesospheric winds at the height of the airglow emissions. The primary goals were (1) to characterize short-period gravity waves over Antarctica and (2) estimate their associated momentum flux [*Espy et al.*, 2004]. The observed quasi-monochromatic gravity wave events from Halley have most recently been reported by *Nielsen et al.* [2009] to exhibit similar characteristics to wave events typically observed at mid- and low-latitudes [*Wu and Killeen*, 1996; *Taylor et al.*, 1997; *Walterscheid et al.*, 1999; *Stockwell and Lowe*, 2001; *Hecht et al.*, 2001,

[1]Computational Physics, Inc., Boulder, Colorado, USA.
[2]Center for Atmospheric and Space Sciences and Department of Physics, Utah State University, Logan, Utah, USA.
[3]British Antarctic Survey, Cambridge, UK.
[4]Now at Department of Physics, Norwegian University of Science and Technology, Trondheim, Norway.
[5]Center for Atmospheric Sciences, Hampton University, Hampton, Virginia, USA.

0148-0227/12/2011JD016261

2004; *Ejiri et al.*, 2003; *Medeiros et al.*, 2003; *Nakamura et al.*, 2003; *Suzuki et al.*, 2004; *Pautet et al.*, 2005].

[4] *Espy et al.* [2004] have also applied a spectral method to investigate momentum flux associated with the ensemble of gravity waves observed from Halley using a method developed by *Gardner et al.* [1999]. They estimated the nightly averaged momentum flux using the Na airglow imager data during the 2000 and 2001 austral winter seasons. This spectral method assumed that all the detected waves were freely propagating and so provided an upper limit to the momentum flux.

[5] Freely propagating gravity waves of tropospheric origin observed in the mesosphere have a horizontal range of typically a few hundred kilometers from the source to their intersection with the OH layer [*Taylor and Henriksen*, 1989]. However, short-period gravity waves (of horizontal wavelengths typically less than ~20 km) have been shown to be prone to ducted motions resulting in horizontal wave propagation over much longer distances [*Isler et al.*, 1997; *Walterscheid et al.*, 1999; *Hecht et al.*, 2001, 2004; *Pautet et al.*, 2005]. Ducting of gravity waves can be caused either by favorable structure in the wind field (Doppler ducting) or in the background temperature profile (thermal ducting) [e.g., *Fritts and Yuan*, 1989]. In the case of Doppler ducting, wind shear and curvature of the wind field can provide favorable conditions for ducting, whereas the thermal ducted region is a result of variation of the Brunt-Väisälä frequency. In particular, Doppler ducting is most favorable when there is a maximum in the wind field in the direction of wave propagation [e.g., *Chimonas and Hines*, 1986; *Wang and Tuan*, 1988; *Isler et al.*, 1997]. Hence Doppler ducting is highly sensitive to the propagation direction of the wave and the background wind field, while thermal ducting is isotropic.

[6] For example, *Isler et al.* [1997] investigated Doppler ducting of short-period gravity waves over Maui (21°N) as part of the CADRE/ALOHA-93 campaign and determined a large fraction (up to ~75%) of the observed waves were Doppler ducted during this limited campaign period in fall 1993. Airglow observations of gravity wave propagation over Adelaide, Australia (35°S) were investigated by *Walterscheid et al.* [1999] and in this case a large fraction were found to be thermally ducted. Similarly, *Hecht et al.* [2001] investigated a number of gravity waves over Urbana, Illinois (40°N), which, like the results of *Walterscheid et al.* [1999], suggested significant thermal ducting. In contrast, *Ejiri et al.* [2003] considered both Doppler and thermal ducting of gravity waves observed over two sites in Japan (35°N and 44°N) and concluded that Doppler ducting was more limited in effect, due to the variable nature of the wind field, whereas thermal ducting was suggested to be important.

[7] Very few observations of short-period gravity waves exist at high-latitudes, most probably due to contamination of the weak airglow emissions by aurora, but also due to the lack of good observing sites [e.g., *Clairemidi et al.*, 1985; *Taylor and Henriksen*, 1989; *Nielsen et al.*, 2006]. As part of the MaCWAVE campaign conducted from Esrange, Sweden (68°N) during winter 2003, a limited number of case studies (5 events) were all found to be freely propagating [*Nielsen et al.*, 2006]. This was due primarily to the relatively weak prevailing wind fields as the observed wave structures exhibited similar characteristics to those at mid-latitudes. Although these measurements were limited to just 5 events they suggest the potential frequent presence of freely propagating gravity waves at high winter-time latitudes.

[8] In a separate study utilizing the airglow imaging and IDI data sets used here, *Nielsen et al.* [2009] established a climatology of the observed and intrinsic wave parameters. Furthermore, the study showed that the majority of observed monochromatic gravity waves over Halley exhibited a strong preference for propagation towards the Antarctic continent. These observations suggest dominant source regions for these waves equatorward of Halley.

[9] In this paper we have utilized co-located simultaneous wind measurements to study the propagation nature (i.e., freely propagating, evanescent, or ducted) of our short-period gravity waves. As far as we are aware, this is the first long-term investigation of the wave propagation nature of such waves at high-latitudes. Our findings show a surprising majority of freely propagating waves with rare clear signatures of Doppler ducted motion (~5%). This result is in sharp contrast to the results of *Isler et al.* [1997] and other similar investigations at mid- and low-latitudes where a majority of waves have been shown to be ducted in nature at MLT heights.

2. Instrumentations and Observations

[10] The gravity wave observations were performed using an all-sky (180°) monochromatic imaging system. The system is a compact field instrument similar in performance to USU imagers used on several previous campaigns [e.g., *Taylor et al.*, 1997; *Pautet et al.*, 2005; *Nielsen et al.*, 2006] to study short-period gravity waves. The system is capable of sequentially imaging several different airglow emissions; the NIR OH (715–930 nm) and O_2 (865.5 nm) bands, and the Na (589.2 nm) emission. A sky background measurement at 572.5 nm was also made to monitor for cloud and auroral emissions. The strong OH signal was measured using an exposure time of 15 sec, while the weaker O_2, and Na measurements used 90 and 120 sec, respectively, yielding an overall cadence time ~6 min with an embedded 2-min OH cadence.

[11] Figure 1 shows an example of complex mesospheric dynamics, exhibiting both billow–like (instabilities) (Figure 1a) and band–like (gravity waves) (Figure 1b) structures measured in the OH airglow emission on 7 June 2000. The wave structures lasted from tens of minutes (instabilities) to several hours (band) and at times filled the instruments field of view. Figure 1a illustrates one of the obstacles of observing the faint airglow at high latitudes as auroral activity is present in lower half of the image. The bright region to the left is the dawn twilight.

[12] The Halley IDI is a NOAA HF ionospheric sounder [*Grubb*, 1979] operating as an imaging Doppler interferometer [*Adams et al.*, 1985, 1986] and has been described in detail elsewhere [*Jones et al.*, 1997; *Charles and Jones*, 1999]. Briefly, this system transmits a 2.75 MHz, 30 μs half–width gaussian pulse using a log-periodic antenna with soundings every 5 min. Signals returned from variations in the refractive index of the atmosphere are range-gated into 5 km bins between 50 and 105 km. For our investigation the data analysis was restricted to the 75 to 95 km (lower

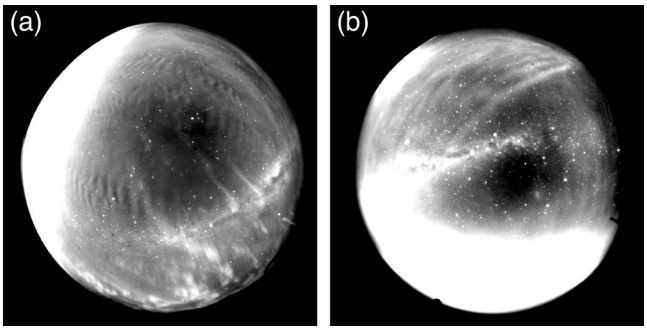

Figure 1. (a) Instability and (b) gravity wave structures measured in the OH airglow emission on 7 June 2000 at 09:25 UT (Figure 1a) and 22:00 UT (Figure 1b), respectively. The images illustrate some of the difficulties with high latitude airglow imaging as evident by the auroral activity present in the lower part of the image. The bright regions to the left (Figure 1a) and bottom (Figure 1b) are the due to the sun.

boundaries in the 5 km altitude bins) region from which the majority of echoes were returned [*Hibbins et al.*, 2006]. The 3-D location of each individual scattering point was determined interferometrically after Doppler sorting of the echoes, and the skymap locations and Doppler velocities of the scattering points were used to fit a mean 3-D velocity vector representative of the motion of the background neutral wind as a function of altitude [*Jones et al.*, 1997]. Mean winds determined by the IDI technique have been calibrated against a meteor radar using a similar Dynasonde operating at Bear Lake Observatory [*Jones et al.*, 2003]. The resulting velocities were found to agree to within 10% magnitude with the IDI returning consistently weaker winds than those recorded by the meteor radar over their common altitude range (80–95 km). Importantly, no systematic decrease in the agreement between the two techniques was observed with increasing height, and no statistically significant variation in the agreement between the two techniques was observed during day and night time operation. Thus the IDI provides reliable information for this initial investigation of the propagation nature of gravity waves over Antarctica. Due to the relative long duration of our observed waves (typically >3 hours) we are using hourly averaged wind fields in our analyses.

[13] One example of a hourly averaged wind profile of zonal (solid) and meridional (dashed) wind fields is shown in Figure 2. The IDI wind measurements are represented by circles, while the line profile is the resulting cubic spline interpolations, which is utilized to estimate the vertical wavelengths of the individual wave events. This particular wind profile was obtained during the time of the wave events shown in Figure 1. Both meridional and zonal wind profiles exhibit a clear vertical wave–like structure with a vertical wavelength of ∼20–30 km.

[14] The CCD imager was used to identify spatially extensive wave events that exhibited lifetimes from ∼30 minutes to the entire length of the observation night as in previous studies [e.g., *Taylor et al.*, 1997; *Pautet et al.*, 2005; *Nielsen et al.*, 2006]. The instrument operated on 281 nights from March through September during the two winter seasons 2000 and 2001, logging a total of 3057 hours of observations with 1376 hours of clear sky suitable for our investigation of gravity waves. Throughout the observation period, a total of 935 (∼68%) hours of airglow data exhibited short–period gravity motion. Figure 3 shows the seasonal distribution of clear sky observations (black) and wave presence (gray) with the percentage of wave observations shown above each month for the two years combined. It is evident that during the main observation season, a significant fraction of clear skies exhibit wave dynamics (66–84%). In total, 276 wave events were observed with 229 events exhibiting a coherent wave pattern suitable for spectral imaging analysis. Of these, coincident wind data spanning the airglow region were available for 171 events.

3. Analysis and Results

[15] In a previous analysis, *Nielsen et al.* [2009] characterized the observed and intrinsic wave parameters for individual wave events measured during the 2000 and 2001 austral winter seasons. The observed horizontal wave parameters (wavelength, phase speed, and propagation direction) were determined using standard spectral and spatial mapping techniques [e.g., *Garcia et al.*, 1997; *Coble et al.*, 1998; *Pautet et al.*, 2005], while the intrinsic wave parameters were calculated using the interpolated background wind. The wind data, taken as hourly averages to reduce measurement uncertainty, had a height resolution of 5 km and were projected onto the wave propagation direction for each wave event. The intrinsic horizontal phase speed is defined as $c_i = c - u_0$, where c is the observed horizontal phase speed and u_0 is the horizontal background wind field in the direction of wave propagation (positive in the wave propagation direction). The intrinsic period (τ_i) is given by $\frac{\lambda_h}{c_i}$ where λ_h is the measured horizontal wavelength.

[16] For each wave event, the observed wave parameters were estimated using 4–8 successive images corresponding

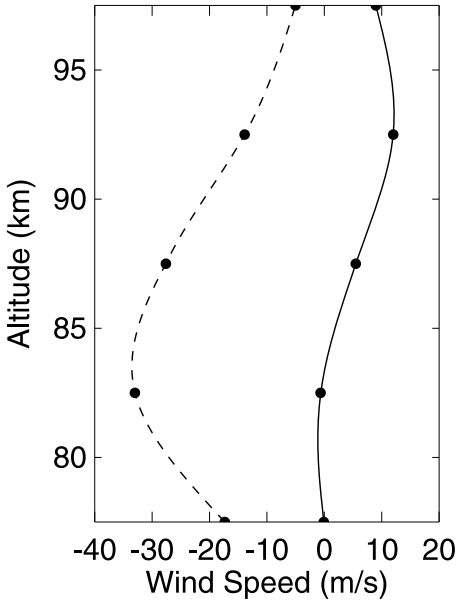

Figure 2. The hourly averaged zonal (solid) and meridional (dashed) wind fields on 7 June 2000, coincident with the dynamics shown in Figure 1.

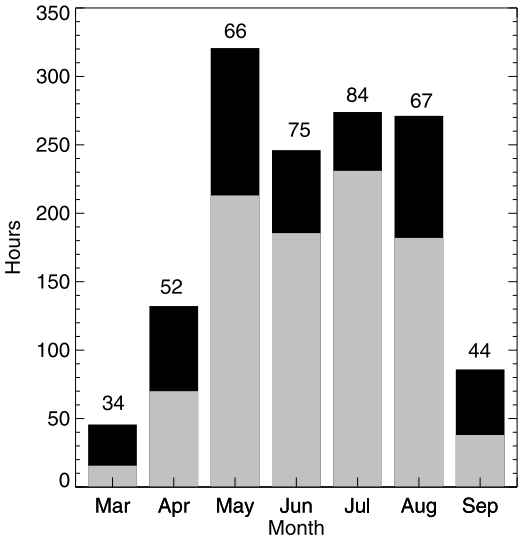

Figure 3. The seasonal distribution of the hourly amount of clear skies (black) and skies exhibiting wave motion (gray). The percentage of observations exhibiting wave motion, with respect to total hours of clear skies, is shown above each bar.

to a ~25–50 minute time period. The nearest coincident hourly averaged wind profile was then used to estimate the intrinsic wave parameters. This process was repeated for each additional hour the wave event was observed followed by averaging of the intrinsic wave parameters.

[17] Over the combined 2000 and 2001 seasons, the observed wave parameters were found to exhibit characteristics similar to those reported from other latitudes, with interquartile range (IQR) spanning from 18–34 km, 34–65 m/s, and 7–12 min for the horizontal wavelength, phase speed, and period, with median values of 25 km, 48 m/s, and 10 min, respectively. The corresponding intrinsic parameters exhibited typical values, similar to the observed parameters, with IQR c_i = 37–68 m/s (median value of 53 m/s) and τ_i = 6–11 min with a median value of 9 min. In the study presented here, the intrinsic phase speeds are utilized to address the vertical propagation characteristics of the observed waves.

[18] The gravity wave propagation nature can be assessed by considering the vertical wavenumber, m, which can be written as [e.g., *Nappo*, 2002]:

$$m^2 = \frac{N^2}{c_i^2} + \frac{u''_0}{c_i} - \frac{1}{H_s}\frac{u'_0}{c_i} - \frac{1}{4H_s^2} - k^2 \quad (1)$$

where N is the Brunt-Väisälä frequency, c_i is the intrinsic phase speed, u_0 is the background wind in the wave direction, H_s is the scale height, k is the horizontal wavenumber, and primes denotes the derivative with respect to altitude. In this equation, the Brunt-Väisälä frequency was calculated using:

$$N^2 = \frac{g}{T}\left(\frac{dT}{dz} + \Gamma\right) \quad (2)$$

where g = 9.54 m/s^2, T is the temperature, $\frac{dT}{dz}$ is the local temperature gradient, and the adiabatic lapse rate is given by Γ = 9.5 K/km. The scale height was found using:

$$H_s = \frac{RT}{g} \quad (3)$$

where R = 287 J· kg^{-1} · K^{-1} is the gas constant for the atmosphere below the turbopause.

[19] Mesospheric temperature profile data are not available for the period of interest from Halley. However, *Nielsen et al.* [2006] performed a similar type of investigation at high northern latitudes using MSIS-90 model temperature data and coincident Na lidar temperature data for five case studies. The two temperature data sets yielded very similar results suggesting that the MSIS-90 model data were quite acceptable for this type of study in the absence of direct temperature measurements. In support of this argument, *Gardner et al.* [2001] showed that the MLT temperature profile over the South Pole measured using a Fe-Boltzman lidar was also quite consistent with the MSIS-90 model. Based on these results we have used the MSIS-90 temperature model to evaluate the Brunt-Väisälä frequency and the scale height.

[20] To best estimate the shear and curvature in the wind field in the vertical direction, a cubic-spline interpolation was applied to the wind data to obtain a smoothly varying profile encompassing the airglow region (75–95 km). The vertical wave number squared (m^2) was then calculated as a function of altitude and a Gaussian weighting (FWHM = 8 km) was applied to estimate the average values appropriate for the OH emission layer centered at 87 km.

[21] The propagation characteristics were then evaluated based on three criteria [*Isler et al.*, 1997]: If $m^2 > 0$ throughout the MLT region the wave was freely propagating. Furthermore, if the vertical wavelength is greater than the thickness of the airglow layer (~8 km) the wave structure should readily be observed with the imager. If the vertical wavelength is less than or equal to the layer thickness then cancelation effects are expected to dominate within the airglow layer and wave visibility will be significantly diminished. If $m^2 < 0$ over a significant part of the MLT region, the wave will be evanescent and its amplitude will decay exponentially with height. If a freely propagating region $m^2 > 0$ was present and bounded by evanescent regions below and above, then the wave may have been ducted. Under these conditions a free-standing wave can propagate large horizontal distances with little attenuation, especially if the wave was tuned to the size of the duct, that is, if the half-integer number of the vertical wavelength was comparable to the duct depth [e.g., *Hecht et al.*, 2001].

[22] The above procedure has been applied to all wave events, with coincident wind measurements, observed over Halley during 2000 and 2001. Waves encountering a critical level ($c_i \rightarrow 0$) within the airglow layer (a total of 7 events) required further, more careful consideration due to singularities in the equation governing the vertical wave number and are not included in this statistical study (leaving 164 wave events for comparison study). The waves were classified according to their dominant propagation characteristic during their observed lifetime.

[23] The results of this analysis show that the majority of the events were found to be freely propagating (80%) throughout the MLT region, while the remaining events

Table 1. Propagation Nature Listed in Percentage for the Two Years of Observations

Year	Freely Propagating	Evanescent	Doppler Ducted	Number of Events
2000	82%	15%	3%	121
2001	77%	14%	9%	43

were determined to be either evanescent (15%) or Doppler ducted (5%) in nature. Table 1 summarizes the propagation nature for the two years of measurements. Figure 4 shows the statistical distribution of vertical wavelengths (skewed right) accumulated over the two observation seasons. The freely propagating waves exhibited vertical wavelengths with a median vertical wavelength (λ_z) of 21 km and IQR of 32 km (first and third quartiles with values of 16 km and 48 km, respectively).

[24] An example for a freely propagating wave occurring on 4 June 2000 is shown in Figure 5 where Figure 5 (left) shows the smoothed vertical profile of horizontal wind, while Figure 5 (middle) displays the vertical wavenumber squared as a function of altitude. Figure 5 (right) shows a snapshot of the OH wave field during this period. Since m^2 is positive throughout the airglow region, this wave was, per definition, freely propagating within this region. The specific wave parameters for this event were λ_h = 25 km, c = 33 m/s, τ = 13 min, λ_z = 10 km, c_i = 26 m/s, while the intrinsic period was determined to be 16 min.

[25] In contrast, Figure 6 shows a similarly presented plot but for an evanescent wave event (observed on 8 June 2000) where the vertical wavenumber squared was negative throughout the airglow layer. This event was characterized by λ_h = 15 km, c = 68 m/s, and τ = 3.7 min. The intrinsic parameters were determined to be c_i = 90 m/s and τ_i = 2.8 min, respectively. Evanescent waves are per definition not vertically propagating ($m^2 < 0$) and the vertical wavelengths are not defined for these waves.

[26] Figure 7 shows profiles for a wave event that suggests a Doppler ducted motion. The wind field (Figure 7, left) exhibits a wind jet in the direction of wave propagation, which is a favorable condition to create a Doppler duct [e.g., *Chimonas and Hines*, 1986; *Isler et al.*, 1997]. Indeed, the vertical wavenumber squared (Figure 7, middle) indicates a possible ducted motion where a freely propagating region is bounded above and below by evanescent regions. In this case, the vertical wavelength was estimated to be ~44 km and the depth of the duct was ~20 km, close to the half-integer of the vertical wavelength (22 km). Thus, the wave was fairly well tuned to propagate inside the duct, with some expected leakage of its energy. The observed wave parameters were λ_h = 17 km, c = 29 m/s, and τ = 9.8 min. The intrinsic parameters were c_i = 44 m/s and τ_i = 6.4 min, respectively. Table 2 lists the wave parameters for the observed waves exhibiting a clear Doppler ducted signature of which there were only eight events.

4. Discussion

[27] One difficulty with the vertical wavenumber analysis is to obtain a good estimate for the wind curvature and shear (second and third term, respectively, in equation (1)). In previous studies, it has been customary to neglect these terms, that is, to assume zero or little wind shear [e.g., *Walterscheid et al.*, 1999; *Ejiri et al.*, 2001, 2003]. For comparison, we have therefore performed the analysis using the "full model" as given by equation (1) and a simplified model neglecting the wind shear and curvature. The simplified dispersion relation is:

$$m^2 = \frac{N^2}{c_i^2} - \frac{1}{4H_s^2} - k^2. \quad (4)$$

[28] The vertical wavelengths estimated using the two dispersion relations agreed on 51 occasions, while they agree within 10% on 102 wave events (out of 164). This result suggests that the curvature and shear in the wind field is not a big factor at least at the resolution available by the radar. The propagation nature of individual waves yielded similar results for all but five of the measured wave events. Thus, determining if a wave was freely propagating, evanescent, or Doppler ducted did not, to a large degree, depend on the dispersion relation used (this was also observed in the work by *Isler et al.* [1997]). The largest discrepancy between the two methods shows up in the quantitative calculation of the vertical wavelength. The values typically agree within 10% but in few cases they can vary as much as 100%. These disagreements occur when the wind fields have a strong shear or exhibit deep maximum/minimum in the vicinity of the airglow layer. This is to be expected since these gradients/curvatures are neglected in the simple model. It should also be noted that where strong wind shears or curvatures occur, the WBK approximation applied in obtaining equation (1) is not valid [e.g., *Nappo*, 2002] and care must be taken in interpreting the results for these few cases. This said, the simple model aids in a graphical method to estimate the limits between evanescent waves and freely propagating or ducted waves. The method was employed by *Swenson et al.* [2000] to study dispersion limits on gravity waves observed in the OH airglow emission. Their study included the two limiting branches obtained from the simplified dispersion relation: one branch separating freely propagating and evanescent waves, when the vertical wavelength approaches infinity (i.e., vertical wave number tends to zero), and one branch set by the detection limit of the instrument (due to the finite thickness of the airglow layer).

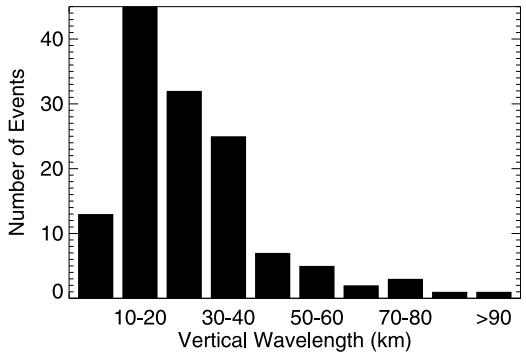

Figure 4. The vertical wavelength distribution for both the 2000 and 2001 seasons. The majority of the waves exhibit vertical wavelengths greater than 10 km and hence are not subject to cancelation effects within the airglow emission.

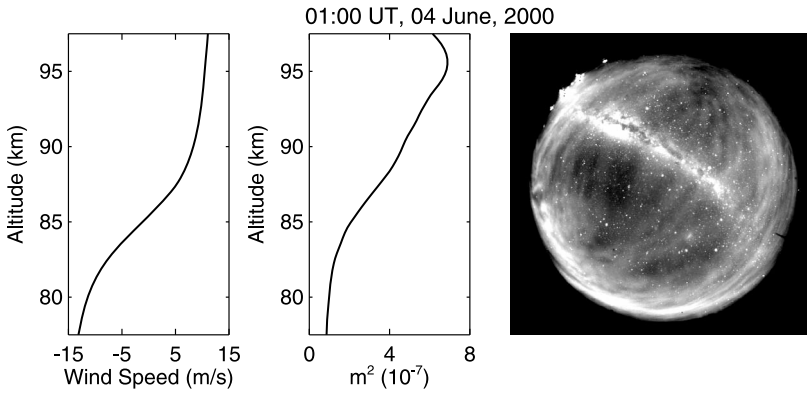

Figure 5. (left) The horizontal wind in wave direction as a function of altitude. (middle) The vertical wavenumber squared. (right) An OH snapshot of the wave field during these conditions. In this particular case, the wave is freely propagating.

[29] The detection of mesospheric gravity waves within the airglow layer is limited to the finite depth of that layer. If the vertical wavelength is greater than the emission layer thickness, the wave can easily be detected with the imager. If the vertical wavelength is less it will experience cancelation effects and may not be detected [*Swenson and Gardner*, 1998]. A typical OH layer thickness is ~8 km (FWHM) and is used as a lower limit in this case.

[30] Figure 8 shows a plot with the two limiting branches where we have assumed a Brunt-Väisälä period of 5 min and a scale height of 6 km. Also shown in the figure are branches corresponding to vertical wavelengths of 20, 40, and 60 km, respectively. Superimposed on this plot are the individual wave events observed during the two seasons calculated using the "full model." The waves above the $m = 0$ branch correspond to events identified as evanescent waves, while it is clear that the majority of events fall within the freely propagating range. Events shown as blue circles are waves that exhibited a clear Doppler ducted signature. It is evident that the favorable location for Doppler ducted waves does indeed occur at relatively short horizontal wavelengths as suggested by *Isler et al.* [1997].

[31] It is possible for the imager to observe waves with lower vertical wavelengths than our imposed limit (< 8 km) if cancelation effects are weak. Furthermore, waves encountering a critical level within the airglow region will naturally exhibit a very low intrinsic phase speed. As a result, the Gaussian averaged intrinsic phase speed may well be under-estimated and the wave will appear below the theoretical observation limit in Figure 8.

[32] The equation governing Doppler or thermal ducting (equation (1) and in simplified form equation (4)) has been used to investigate the effects of background winds on the propagation of the waves at MLT heights. The majority of the waves (~80%) were found to be freely propagating in the airglow region. This result could have profound influences on our comprehension and impact of short-period gravity waves at high latitudes. *Espy et al.* [2004, 2006] calculated an upper limit to the vertical transport of horizontal momentum flux assuming all the waves to be freely propagating. They used an automated algorithm to detect wave activity due to an ensemble of waves (that did not identify individual events) and then estimated the momentum flux using the method by *Gardner et al.* [1999]. However, as we have shown, it is important first to establish the propagation nature of the waves in order to accurately assess their potential impact on the upper atmosphere. The results found in our Doppler ducting investigation support the assumption made by *Espy et al.* [2004] that the majority of

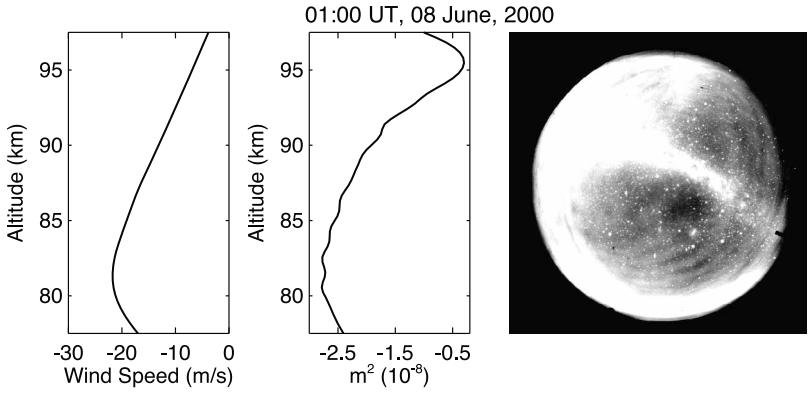

Figure 6. Similar to Figure 5, but the vertical wavenumber is imaginary, and the wave is evanescent within the region shown.

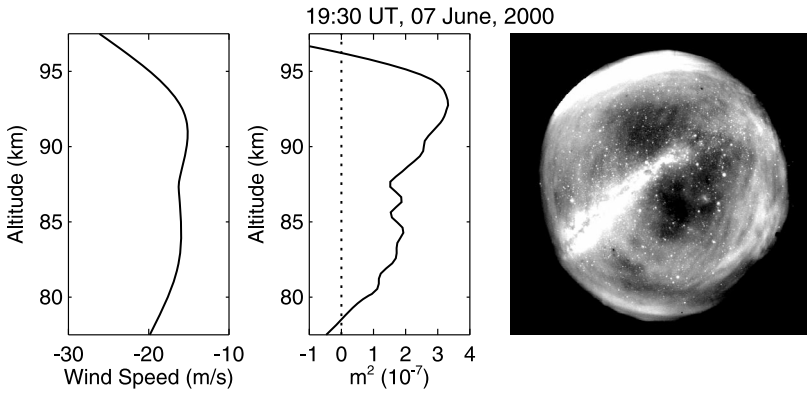

Figure 7. Similar to Figures 5 and 6, showing a freely propagating region ($m^2 > 0$) bounded by evanescent regions above and below, creating a Doppler ducted region between from ~77–97 km. Notice the jet in the wind profile, which is a favorable condition for Doppler ducting.

the waves are freely propagating but the effects of thermal ducting over Antarctica remain unanswered.

[33] Thermal and Doppler ducting of short-period gravity waves are common at mid- and low-latitudes [e.g., *Isler et al.*, 1997; *Walterscheid et al.*, 1999; *Hecht et al.*, 2001]. However, the full importance of ducted wave motion at high latitudes has previously not been established. The results obtained in this analysis suggest the majority of the observed waves to be freely propagating with only ~5% showing a clear Doppler ducted signature. As mentioned earlier, a wave can be Doppler ducted if a freely propagating region is bounded above and below by evanescent regions. However, there are some considerations to take into account regarding the evanescent regions. If the wave is to reach the ducting level the evanescent regions cannot be vertically extensive or they will be severely damped. The depth of the evanescent regions for these events are difficult to estimate from the available wind data due to the lower boundary of 75 km.

[34] The low number of Doppler ducted waves in our study is in sharp contrast to studies at mid latitudes where Doppler ducting plays a significant role in wave propagation. The answer to this discrepancy may be explained with a consideration of the wind field. In the altitude region where these observations were made, wind field above Halley has shown to be relatively weak with magnitudes <10 m/s [*Hibbins et al.*, 2006; *Nielsen et al.*, 2009]. Furthermore, *Hibbins et al.* [2007] reported similar weak winds over Rothera (67° S) located on the Antarctic Peninsula. This is in contrast to wind fields at mid latitudes which appear stronger in magnitude [e.g., *Hagan et al.*, 1999; *Zhang et al.*, 2003] and may explain the larger number of Doppler ducted waves at those latitudes. In particular, *Snively et al.* [2007] showed how strong tidal winds (peak winds >60 m/s) over Bear Lake, Utah (42°N) are providing support for a Doppler ducted wave motion. *Murphy et al.* [2006] analyzed multiple years of wind data from 8 sites distributed on the Antarctic continent to obtain a latitude-longitude-height variation of tidal winds over the whole continent. Their study revealed that the winds exhibited typical amplitudes less than those typically observed at mid latitudes.

[35] With the above discussion in mind, the weak wind field observed over Halley suggests that the wind structure is not capable of sustaining Doppler ducted waves. A similar conclusion may be extended to the northern polar region. In support of this idea, is the limited wave observations by *Nielsen et al.* [2006] and Arctic MLT winds by *Portnyagin et al.* [2004]. In their study, *Portnyagin et al.* [2004] utilized a network of MF and meteor radars located at Andenes (69°N), Tromsø(70°N), Esrange (68°N), Dixon (73.5°N),

Table 2. Wave Parameters for the Observed Waves Exhibiting a Clear Doppler Ducted Signature Within the Airglow Region

λ_h (km)	c (m/s)	τ (min)	λ_z (km)	c_i (m/s)	τ_i (min)
18	48	6	39	44	7
17	29	10	44	45	6
19	22	14	11	29	11
35	36	16	15	43	14
18	67	5	20	35	9
17	24	12	20	41	7
33	68	8	39	83	7
14	75	3	23	38	6

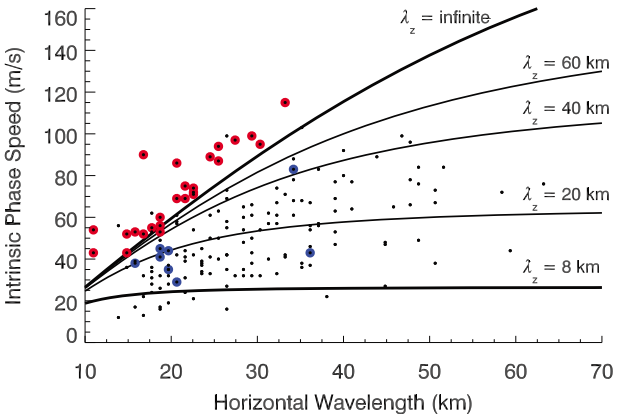

Figure 8. Illustration of the dispersion conditions from equation (4). The two thick solid lines represent the limiting branches for freely propagating waves observable with the airglow imager, while the thin solid lines represent a selection of vertical wavelengths. The blue circles indicate waves that exhibited a clear Doppler ducted signature, while the red circles show evanescent waves.

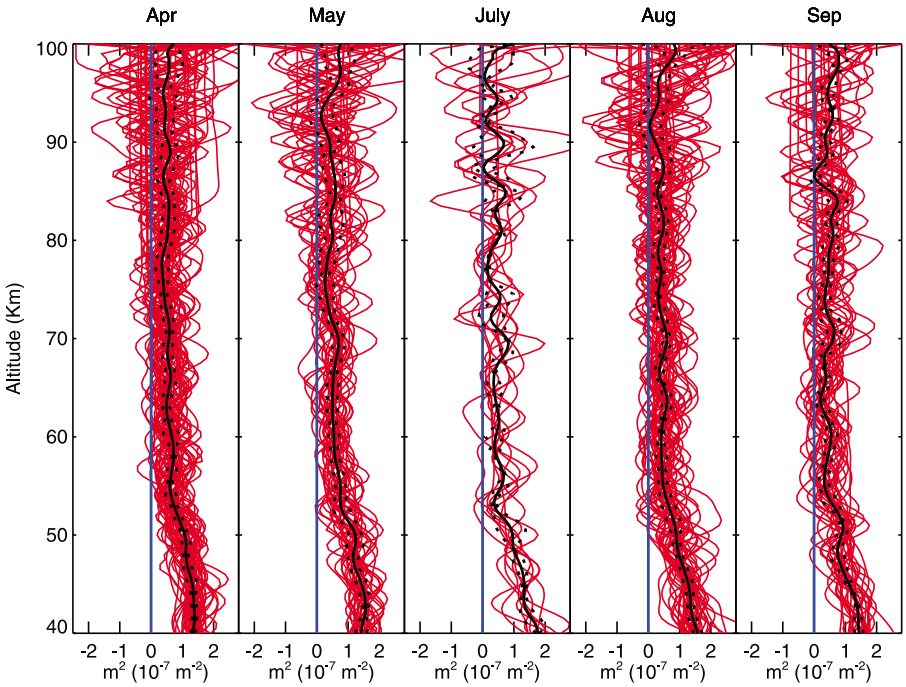

Figure 9. The estimated vertical wavenumbers squared calculated using individual SABER temperature profiles, and median wave parameters. The mean profiles and corresponding standard deviation are shown in solid and dashed black profiles, respectively.

Poker Flat (65°N), and Resolute Bay (75°N). The winds exhibited similar seasonal variations as compared to lower latitudes but with a general weaker amplitudes. The mean winds were similar to those in the southern polar region, typically exhibiting wind speeds <10 m/s and tidal winds <15 m/s (one station exhibited tidal winds up to ~20 m/s during the winter months). *Nielsen et al.* [2006] investigated 5 wave events observed over Esrange, Sweden (68°N) during the winter MaCWAVE campaign and found all 5 events to be freely propagating.

[36] The above support the idea that not only Antarctic, but in general, polar MLT winds are not significant enough to provide support for substantial Doppler ducted motion of short-period gravity waves during the deep winter months where the majority of our observations occur. This conclusion has a profound impact on the mesospheric circulation as the majority of these polar mesospheric waves are likely freely propagating and therefore transporting energy into the MLT region from below. However, we must note that our observations are selective as they represent a small part of a much bigger gravity wave spectrum, limited to night time observations during the polar winter months.

[37] Evanescent waves are damped in the vertical direction (m imaginary) and hence can only travel horizontally. In general, the amplitude of such waves decays exponentially with altitude from the source region. However, as the stability of the atmosphere is changing with height (i.e., stratification), there is a possibility that a freely propagating wave may become evanescent at a given altitude where reflection will then occur [e.g., *Nappo*, 2002]. Furthermore, it is important to note that even though a wave is evanescent, energy can still leak through an evanescent region (an effect termed tunneling [e.g., *Nappo*, 2002]). During the two observation seasons less than a quarter of the events were found to be evanescent at MLT heights.

[38] The role of thermal ducting is difficult to address as coincident temperature measurements are not available from Halley during the 2000 and 2001 observation seasons. In our analysis we utilized the MSIS-90 climatology. However, sporadic presence of mesospheric inversion layers (MIL), which are important for the formation of thermal ducts, are not present in the climatological model.

[39] *Meriwether and Gardner* [2000] and *Cutler et al.* [2001] reported less MILs at high latitudes compared to studies at low and mid–latitudes. In the review paper by *Meriwether and Gerrard* [2004] they speculated on a few causes of the reduction of high–latitude MILs. First, was the lack of high-altitude observations/data analysis. Second, the presence of the polar vortex makes it difficult to identify MILs, and finally, critical layer filtering of gravity waves thought to be necessary for the production of MILs. As our results show, gravity waves are present in high numbers in the Antarctic winter mesosphere over Halley. It is beyond the scope of this paper to investigate the presence of MILs in great detail, particularly in relation to the polar vortex as this is expected to be a complex process. However, since the work by *Meriwether and Gerrard* [2004], the SABER instrument onboard the TIMED mission have completed 9 seasons of temperature measurements, including measurements over the Antarctic region. In order to address the presumptive occurrence rate of MILs over Halley, we have utilized the SABER temperature data set [*Russell et al.*, 1999; *Mertens et al.*, 2004].

[40] The impact of the more realistic temperature profiles (including MILs) on the observed gravity wave field, and hence thermal ducting, can be estimated by considering the

vertical wavenumber squared profiles calculated from equation (4) utilizing the individual SABER temperature profiles. In the calculations, we have used the median horizontal wavelength, observed phase speed, and intrinsic phase speed as a proxy for the observed wave field. The temperature profiles were restricted to profiles occurring within our observation season and within 5° of Halley in latitude and longitude. Furthermore, we restricted the temperature data to profiles with sufficient data points to resolve the thermal structure in the MLT region.

[41] A total of 154 temperature profiles satisfied the above criterions. The subsequent analysis revealed 83 (54%) profiles exhibiting freely propagating conditions throughout the MLT region, 28 (18%) profiles suggested evanescent motion, while 43 (28%) profiles featured a ducted region caused by the thermal structure. Figure 9 shows the corresponding calculated m^2 profiles (red profiles), while the solid black lines show the mean profiles and the standard deviations are shown as dotted black profiles. It is evident that the majority of the profiles exhibit freely propagating nature below 80 km. However, there are few profiles with significant evanescent regions causing both evanescent and thermal ducted propagation conditions. These results suggest that the thermal ducted motion is more prevalent than Doppler ducted motion (5%). Our previous estimate of 80% of the observed wave field exhibiting freely propagating motion (based on climatological temperature field) is most probably an overestimate, as it neglects a significant amount of possible thermal ducted waves. Although inclusion of the SABER temperature profiles reveal a significant amount of potentially thermal ducted waves, the majority of the observed waves still appear to be freely propagating. Analyses using combinations of the lower and upper quartile values of horizontal wavelength and intrinsic phase speed reveal similar results suggesting our conclusion is robust to the variations in our wave parameters.

[42] The sources of the waves observed from Halley have yet to be fully investigated. Our newly acquired knowledge about the propagation nature of gravity waves combined with their preferential direction of propagation [*Nielsen et al.*, 2009] helps identify possible source locations of these Antarctic waves. Strong convective regions do exist over the South Atlantic Ocean and could be a source of long-range (several thousand kilometers) ducted waves over Halley. Since the majority of the observed waves imaged in the MLT region were vertical propagating, these distant convective zones are not likely source candidates. However, there is a possibility that waves generated at large range could be trapped in a lower atmospheric duct only to become freely propagating near Halley. This said, the likelihood that the majority of the observed waves would experience such trapped motion is very small and points towards alternative source regions in the near vicinity of Halley.

[43] Together with the climatological study by *Nielsen et al.* [2009], the study presented here lays the ground work towards an understanding of the sources of these southern polar waves. Application of ray tracing techniques together with satellite imagery and weather maps are needed to help identify these sources, while the extensive lack of middle atmospheric wind and temperature measurements have prohibited such detailed studies, basic ray tracing of gravity waves vertically through a realistic atmosphere in the vicinity of Halley has been carried out by *Lawrence* [2002]. Recent advancement of extending atmospheric numerical weather prediction (NWP) systems into the upper mesospheric region, implies that more detailed studies are now permissible. One such NWP system is the Navy Operational Global Atmospheric Prediction System Advanced Level Physics High Altitude (NOGAPS-ALPHA), which has been extended up to an altitude of ~95 km [*Eckermann et al.*, 2009]. With this new tool, in concert with ray tracing techniques, detailed research into the origin of the dominant sources of gravity waves observed over Halley can now be accomplished.

5. Conclusion

[44] We have investigated intrinsic wave parameters and the propagation nature of short-period mesospheric gravity waves from Halley, Antarctica, over two seasons using simultaneous all-sky airglow imager wave and IDI wind measurements. This is the first study using long-term data to investigate the propagation nature of these waves at high polar latitudes. Similar studies at mid- and low-latitudes have shown that a large fraction of wave events exhibited either Doppler or thermal ducted motions. This is in contrast to our Antarctic findings which indicate the majority of the waves were freely propagating with only ~5% showing a clear Doppler ducted motion. We attribute this marked difference to the relative weak mesospheric wind field over Halley that was not capable of sustaining Doppler ducted motions. Although no coincident temperature measurements were available, ten years of co–located SABER data, suggest that up to 28% of the measured temperature profiles would support thermal ducted wave motion.

[45] Our results support the assumption of *Espy et al.* [2004] that a large fraction of winter–time short-period waves present over Halley were freely propagating. In addition, existing high latitude wind measurements combined with a limited wave propagation study suggest that the polar MLT winds may not be capable of supporting extensive Doppler ducted wave motion of these short-period gravity waves. These high latitude waves are thus an important component in the general circulation as a majority of them are likely to transport energy and momentum from the underlying atmosphere.

[46] Knowledge of the dominant freely propagating nature of these waves, combined with previous observations regarding their preferred propagation direction toward the Antarctic continent, points towards a wave source(s) in the near vicinity but to the north of Halley.

[47] **Acknowledgments.** This research was jointly supported by the UK Natural Environment Research Council (NERC), the National Science Foundation, Office of Polar Programs, under grants OPP-9816465 and OPP-0338364, ATM-0350680, and AGS-1026996.

References

Adams, G. W., D. P. Edwards, and J. W. Brosnahan (1985), The imaging doppler interferometer-data analysis, *Radio Sci.*, *20*(6), 1481–1492.

Adams, G. W., J. W. Brosnahan, D. C. Walden, and S. F. Nerney (1986), Mesospheric observations using a 2.66-MHz radar as an imaging doppler interferometer - description and 1st results, *J. Geophys. Res.*, *91*(A2), 1671–1683.

Charles, J., and G. O. L. Jones (1999), Mesospheric mean winds and tides observed by the Imaging Doppler Interferometer (IDI) at Halley, Antarctica, *J. Atmos. Sol. Terr. Phys.*, *61*(5), 351–362.

Chimonas, G., and C. O. Hines (1986), Doppler ducting of atmospheric gravity waves, *J. Geophys. Res.*, *91*, 1219–1230.

Clairemidi, J., M. Herse, and G. Moreels (1985), Bi-dimensional observations of waves near the mesopause at auroral latitudes, *Planet. Space Sci*, *33*, 1013–1022.

Coble, M. R., C. Papen, and C. S. Gardner (1998), Computing two-dimensional unambiguous horizontal wavenumber spectra from OH airglow images, *IEEE Trans. Geosci. Remote Sens.*, *36*, 368–382.

Cutler, L. J., R. L. Collins, K. Mizutani, and T. Itabe (2001), Rayleigh lidar observations of mesospheric inversion layers at Poker Flat, Alaska (65°N, 147°W), *Geophys. Res. Lett.*, *28*, 1467–1470.

Eckermann, S. D., K. W. Hoppel, L. Coy, J. P. McCormack, D. E. Siskind, K. Nielsen, A. Kochenash, M. H. Stevens, C. R. Englert, and M. E. Hervig (2009), High-altitude data assimilation system experiments for the northern summer mesosphere season of 2007, *J. Atmos. Terr. Phys.*, *71*(3–4), 531–551, doi:10.1016/j.jastp.2008.09.036.

Ejiri, M. K., K. Shiokawa, T. Ogawa, T. Nakamura, R. Maekawa, T. Tsuda, and M. Kubota (2001), Small-scale gravity waves near the mesopause observed by four all-sky airglow images, *J. Geophys. Res.*, *106*(D19), 22,793–22,799.

Ejiri, M. K., K. Shiokawa, T. Ogawa, K. Igarashi, T. Nakamura, and T. Tsuda (2003), Statistical study of short-period gravity waves in OH and OI nightglow images at two separated sites, *J. Geophys. Res.*, *108*(D21), 4679, doi:10.1029/2002JD002795.

Espy, P. J., G. O. L. Jones, G. R. Swenson, J. Tang, and M. J. Taylor (2004), Seasonal variations of the gravity wave momentum flux in the Antarctic mesosphere and lower thermosphere, *J. Geophys. Res.*, *109*, D23109, doi:10.1029/2003JD004446.

Espy, P. J., R. E. Hibbins, G. R. Swenson, J. Tang, M. J. Taylor, D. M. Riggin, and D. C. Fritts (2006), Regional variations of mesospheric gravity–wave momentum flux over Antarctica, *Ann. Geophys.*, *24*, 81–88.

Fritts, D. C., and M. J. Alexander (2003), Gravity wave dynamics and effects in the middle atmosphere, *Rev. Geophys.*, *41*(1), 1003, doi:10.1029/2001RG000106.

Fritts, D. C., and R. A. Vincent (1987), Mesospheric momentum flux studies at Adelaide, Australia: Observations and a gravity wave/tidal interaction model, *J. Atmos. Sci.*, *44*, 605–619.

Fritts, D. C., and L. Yuan (1989), An analysis of gravity wave ducting in the atmosphere: Eckarts resonances in thermal and doppler ducts, *J. Geophys. Res.*, *94*, 18,445–18,466.

Garcia, F. J., M. J. Taylor, and M. C. Kelley (1997), Two-dimensional spectral analysis of mesospheric airglow image data, *Appl. Opt.*, *36*, 7374–7385.

Gardner, C. S., K. Gulati, Y. Zhao, and G. R. Swenson (1999), Measuring gravity wave momentum fluxes with airglow images, *J. Geophys. Res.*, *104*, 1903–1915.

Gardner, C. S., G. C. Papen, X. Chu, and W. Pan (2001), First lidar observations of middle atmopshere temperature, Fe densities, and polar mesopsheric clouds over the north and south poles, *Geophys. Res. Lett.*, *28*(7), 1199–1202.

Grubb, R. N. (1979), The NOAA SEL HF radar system (ionospheric sounder), *Tech. Memo. ERL-SEL 55*, Natl. Oceanic and Atmos. Admin., Silver Spring, Md.

Hagan, M. E., M. D. Burrage, J. M. Forbes, J. Hackney, W. J. Randel, X. Zhang (1999), GSWM-98: Resulst for migrating solar tides, *J. Geophys. Res.*, *104*(A4), 6813–6827.

Hecht, J. H., R. L. Walterscheid, M. Hickey, and S. Franke (2001), Climatology and modeling of quasi-monochromatic atmospheric gravity waves observed over Urbana, Illinois, *J. Geophys. Res.*, *106*(D6), 5181–5196.

Hecht, J. H., S. Kovalam, P. T. May, G. Mills, R. A. Vincent, R. L. Walterscheid, and J. Woithe (2004), Airglow imager observations of atmospheric gravity waves at Alice Springs and Adelaide, Australia during the Darwin Area Wave Experiment (DAWEX), *J. Geophys. Res.*, *109*, D20S05, doi:10.1029/2004JD004697.

Hibbins, R. E., P. J. Espy, and M. J. Jarvis (2006), Mean winds and tides in the mesosphere and lower thermosphere above Halley, Antarctica, *J. Atmos. Terr. Phys.*, *68*(3–5), 436–444.

Hibbins, R. E., P. J. Espy, M. J. Jarvis, D. M. Riggin, and D. C. Fritts (2007), A climatology of tides and gravity wave variance in the MLT above Rothera, Antarctica obtained by MF radar, *J. Atmos. Terr. Phys.*, *69*(4–5), 578–588.

Isler, J. R., M. J. Taylor, and D. C. Fritts (1997), Observational evidence of wave ducting and evanescence in the mesosphere, *J. Geophys. Res.*, *102*, 26,301–26,313.

Jones, G. O. L., K. Charles, and M. J. Jarvis (1997), First mesospheric observations using an imaging Doppler interferometer adaption of the dynasonde at Halley, Antarctica, *Radio Sci.*, *32*(6), 2109–2122.

Jones, G. O. L., F. T. Berkey, C. S. Fish, W. K. Hocking, and M. J. Taylor (2003), Validation of imaging Doppler interferometer winds using meteor radar, *Geophys. Res. Lett.*, *30*(4), 1743, doi:10.1029/2003GL017645.

Lawrence, A. R. (2002), Observation of vertically propagating atmospheric waves above Antarctica, PhD thesis, Univ. of Cambridge, Cambridge, U. K.

Medeiros, A. F., M. J. Taylor, H. Takahashi, P. P. Batista, and D. Gobbi (2003), An investigation of gravity wave activity in the lower-latitude upper mesopause: Propagation direction and wind filetering, *J. Geophys. Res.*, *108*(D14), 4411, doi:10.1029/2002JD002593.

Meriwether, J. W., and C. S. Gardner (2000), A review of the mesospheric inversion layer phenomenon, *J. Geophys. Res.*, *105*, 12,405–12,416, doi:10.1029/2002JD002593.

Meriwether, J. W., and A. J. Gerrard (2004), Mesospheric inversion layers and stratospheric temperature enhancements, *Rev. Geophys.*, *42*, RG3003, doi:10.1029/2003RG000133.

Mertens, C. J., et al. (2004), SABER observations of mesospheric temperatures and comparisons with falling sphere measurements taken during the 2002 Summer MaCWAVE campaign, *Geophys. Res. Lett.*, *31*, L03105, doi:10.1029/2003GL018605.

Murphy, D. J., et al. (2006), A climatology of tides in the Antarctic mesosphere and lower thermosphere, *J. Geophys. Res.*, *111*, D23104, doi:10.1029/2005JD006803.

Nakamura, T., T. Aono, T. Tsuda, A. G. Admiranto, E. Achmad, and Suranto (2003), Mesospheric gravity waves over a tropical convective region observed by OH airglow imaging in Indonesia, *Geophys. Res. Lett.*, *30*(17), 1882, doi:10.1029/2003GL017619.

Nappo, C. J. (Ed.) (2002), *Atmospheric Gravity Waves*, *Int. Geophys. Ser.*, vol. 85, Academic, San Diego, Calif.

Nielsen, K., M. J. Taylor, P. D. Pautet, D. C. Fritts, N. Mitchell, C. Beldon, B. P. Williams, W. Singer, F. J. Schmidlin, and R. A. Goldberg (2006), Propagation of short-period gravity waves at high-latitudes during the MaCWAVE winter campaign, *Ann. Geophys.*, *24*, 1227–1243.

Nielsen, K., M. J. Taylor, R. E. Hibbins, and M. J. Jarvis (2009), Climatology of short-period mesospheric gravity waves over Halley, Antarctica (76°S, 27°W), *J. Atmos. Terr. Phys.*, *71*, 999–1000.

Pautet, P., M. J. Taylor, A. Z. Liu, and G. R. Swenson (2005), Climatology of shot-period gravity waves observed over Northern Australia during the Darwin Area Wave Experiment (DAWEX) and their dominant source regions, *J. Geophys. Res.*, *110*, D03S90, doi:10.1029/2004JD004954.

Portnyagin, Y. I., et al. (2004), Monthly mean climatology of the prevailing winds and tides in the Arctic mesosphere/lower thermosphere, *Ann. Geophys.*, *22*, 3395–3410.

Russell, J. M., III, M. G. Mlyncsak, L. L. Gordley, J. Tansock, and R. Esplin (1999), An overview of the SABER experiment and preliminary calibration results, *Proc. SPIE*, *3756*, 277–288.

Snively, J. B., V. P. Pasko, M. J. Taylor, and W. K. Hocking (2007), Doppler ducting of short-period gravity waves by midlatitude tidal wind structure, *J. Geophys. Res.*, *112*, A03304, doi:10.1029/2006JA011895.

Stockwell, R. G., and R. P. Lowe (2001), Airglow imaging of gravity waves: 1. Results from a small network of OH nightglow scanning imagers, *J. Geophys. Res.*, *106*(D15), 17,185–17,203.

Suzuki, S., K. Shiokawa, Y. Otsuka, T. Ogawa, and P. Wilkinson (2004), Statistical characteristics of gravity waves observed by an all-sky imager at Darwin, Australia, *J. Geophys. Res.*, *109*, D20S07, doi:10.1029/2003JD004336.

Swenson, G. R., and C. S. Gardner (1998), Analytical models for the response of the mesospheric OH* and Na layers to atmospheric gravity waves, *J. Geophys. Res.*, *103*(D6), 6271–6294.

Swenson, G. R., M. J. Alexander, and R. Haque (2000), Dispersion imposed limits on atmospheric gravity waves in the mesosphere: Observations form OH airglow, *Geophys. Res. Lett.*, *27*(6), 875–878.

Taylor, M. J., and K. Henriksen (1989), Gravity wave studies at polar latitudes, in *Electromagnetic Coupling in the Polar Clefts and Caps*, edited by P. E. Sandholt and A. Egeland, pp. 421–434, Springer, New York.

Taylor, M. J., W. R. Pendleton Jr., S. Clark, H. Takahashi, D. Gobbi, and R. A. Goldberg (1997), Image measurements of short-period gravity waves at equatorial latitudes, *J. Geophys. Res.*, *102*, 26,283.

Walterscheid, R. L., J. H. Hecht, R. A. Vincent, I. M. Reid, J. Woithe, and M. P. Hickey (1999), Analysis and interpretation of airglow and radar observations of quasi-monochromatic gravity waves in the upper mesosphere and lower thermosphere over Adelaide, Australia (35°S, 138°E), *J. Atmos. Sol. Terr. Phys.*, *61*, 461.

Wang, D. Y., and T. F. Tuan (1988), Brunt-Doppler ducting of small-period gravity waves, *J. Geophys. Res.*, *93*, 9916–9926.

Wu, Q., and T. L. Killeen (1996), Seasonal dependence of mesospheric gravity waves (<100 km) at Peach Mountain Observatory, Michigan, *Geophys. Res. Lett.*, *23*, 2211–2214.

Zhang, S. P., L. P. Goncharenko, J. E. Salah, R. G. Roble, and G. G. Shepherd (2003), Climatology of neutral winds in the lower thermosphere over Millstone Hill (42.6°N) observed from the ground and from space, *J. Geophys. Res.*, *108*(A1), 1051, doi:10.1029/2002JA009512.

R. E. Hibbins, Department of Physics, Norwegian University of Science and Technology, N-7491 Trondheim, Norway. (robert.hibbins@ntnu.no)

M. J. Jarvis, British Antarctic Survey, Madingley Road, Cambridge CB3 0ET, UK. (mjja@bas.ac.uk)

K. Nielsen, Computational Physics, Inc., 1650 38th St., Ste. 105W, Boulder, CO 80301, USA. (knielsen@cpi.com)

J. M. Russell III, Center for Atmospheric Sciences, Hampton University, 23 Tyler St., Hampton, VA 23668, USA. (james.russell@hamptonu.edu)

M. J. Taylor, Department of Physics, Utah State University, Logan, UT 84322, USA. (mike.taylor@usu.edu)